Design and Crystallographic Screening of a Highly Sociable and Diverse Fragment Library Towards Novel Antituberculotic Drugs

Philipp Janssen[1§], Fabrice Becker[1,2§], Friederike T. Füsser[1,2], Nataliya Tolmachova[3], Tetiana Matviiuk[3,4], Ivan Kondratov[3,5,6], Manfred S. Weiss[7], Daniel Kümmel[2], ***Oliver Koch***[1*]

[1]Institute of Pharmaceutical and Medicinal Chemistry, University of Münster, Germany; [2]Institute of Biochemistry, University of Münster, Germany; [3]Enamine Ltd., Kyiv, Ukraine; [4]HSPH, Harvard University, MA, USA; [5]Enamine Germany GmbH, Frankfurt am Main., Germany; [6]V. P. Kukhar Institute of Bioorganic Chemistry and Petrochemistry, National Academy of Sciences of Ukraine, Kyiv, Ukraine; [7]Macromolecular Crystallography, Helmholtz-Zentrum Berlin, Germany

§Equally Contributing Authors

*Corresponding author
Institute of Pharmaceutical and Medicinal Chemistry, University of Münster
Corrensstraße 48, 48149 Münster
Homepage: www.kochlab.org, Email: oliver.koch@uni.muenster.de

Abstract

Missing synthetic tractability is a common pitfall that is often impeding fragment-to-lead campaigns. Ideally, the follow-up fragment extension would be performed quickly and exhaustively, leading to novel hit or lead compounds in rapid succession without the need for tediously developing synthetic methodologies. However, no fragment library currently has this so-called “sociability” as its primary design principle. Herein, we describe the development of a 96-membered, highly diverse, and entirely sociable fragment library suitable for crystallographic screening. Hundreds to thousands of follow-up compounds modified at all growth vectors are available for each fragment from Enamine’s REAL Space. Additionally, tens to hundreds of thousands of larger and more complex leadlike molecules are accessible per library member, further expanded by scaffold-modified, alternative fragments. This allows for rapid exploration of the chemical space around a fragment of interest without much effort. Here, this library was used for a crystallographic fragment screening on a mycobacterial thioredoxin reductase to identify new starting points for developing new anti-tuberculotic agents. Several hits have been identified in a preliminary analysis of the screening.

Introduction

Fragment-based drug discovery (FBDD) is a method for screening and developing small molecules that has gained widespread popularity over the last 25 years in medicinal chemistry.[1] Currently, seven fragment-derived drugs have been approved, and many more are in different clinical stages.[2–9] In contrast to traditional high-throughput screening, FBDD utilises compounds with fewer atoms, allowing for more efficient coverage of the available chemical space.[10] Additionally, the risk for clashes decreases, facilitating highly efficient interactions with the protein.[11] Fragments, however, usually bind only weakly to their target, necessitating sensitive, biophysical screening methods.

As the choice of fragment library can impact the downstream development into a promising lead molecule, these libraries must be designed carefully. Many commercial and academic libraries of various sizes are available, and some are geared towards specific properties and targets.[12] Regardless of choice, a common issue lies in the follow-up to a screening campaign. Once promising hits are discovered, they need to be developed further quickly. However, synthetic challenges often impede this, demanding more time and resources than appropriate.[13] This problem is also mirrored in a poll from Dan Erlanson on his blog “Practical Fragments”.[14] Although not representative, almost three-quarters of the participants could often or sometimes not develop a fragment due to synthetic challenges. Even more concerning is that nearly two-thirds of all participants had complete fragment-to-lead projects often or sometimes impeded by these issues (Figure 1).

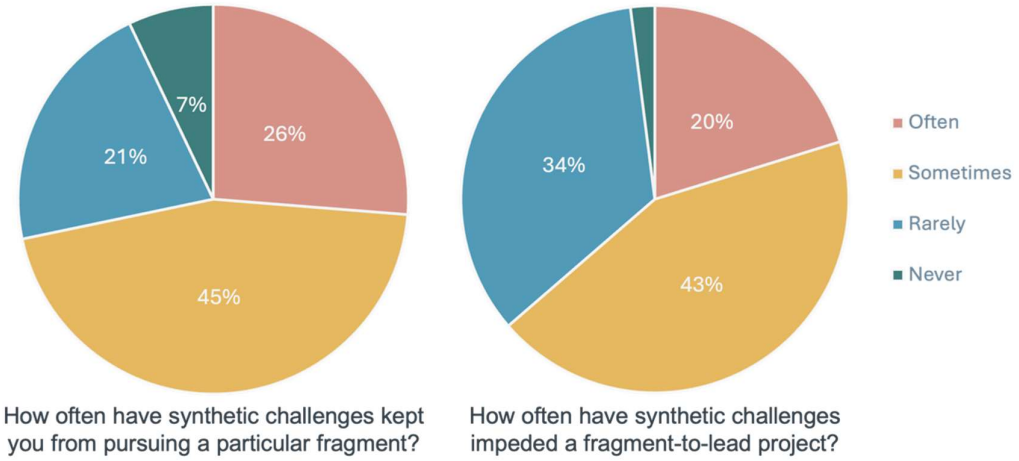

Figure 1: Adapted poll results from “Practical fragments” show a concerning degree of synthetic challenges in fragment to lead projects. The poll was run on the website from 14 June to 16 July 2021. There were forty-two responses to the left question and forty-four responses to the right question.[14]

Regarding this issue, St. Denis et al. roughly classified fragments into two groups during a review of Astex's in-house libraries: sociable and unsociable.[13] Whereas unsociable fragments have barely any accessible growth vectors and few commercial analogues, sociable ones can be developed in nearly all directions with robust chemistry, and large numbers of follow-up compounds are purchasable. The latter are the fragments desired in libraries, but based on the poll results, the former are concerningly widespread. We encountered the issue of unsociability ourselves in the follow-up to one of our crystallographic fragment screens.[15] For a promising fragment, the necessary growth vectors were not accessible, and no buyable compounds modified in the required position were purchasable. The fragment was developed into a novel, potent inhibitor nonetheless, but it needed more time and effort than should have been necessary.[16]

With sociability in mind, we started to look for fragment libraries that address this issue. Fortunately, there is a rising interest in libraries that ease hit development. Cox et al. from the Diamond Light Source developed so-called "poised fragments" consisting of two synthons linked by robust synthetic methodology.[17] This quickly allows scaffold hopping for an identified binder. The concept was further developed by Sreeramulu et al. from the iNEXT initiative.[18] Recently, ChemSpace has launched their "REAL Fragment library", which consists of fragments that can be developed in several directions.[19] Nonetheless, to date, there is no entirely sociable fragment library where a hit can be developed in virtually all directions. However, the recently developed, ultra-large, make-on-demand libraries have made previously unseen chemical spaces accessible and are privileged to be considered when designing new libraries.

Inspired by the design of the F2X-libraries[20], we herein describe the design of a fragment library suitable for crystallographic screening that allows access to virtually all growth vectors. Based on Enamine's REAL Space, hundreds of individually substituted and tens of thousands of larger, leadlike follow-up compounds are available for each fragment. Overall, the 96-fragment core library gives access to over 14 million follow-up compounds in Enamine's REAL Space. A correspondingly higher number of follow-up compounds is available for the 1098 fragment clusters. To prove its usefulness, this fragment library was used for a crystallographic fragment screening on *Mycobacterium smegmatis* thioredoxin reductase (Msm-TrxR). Due to a high sequence identity, this enzyme serves as a model for its homologue in *Mycobacterium tuberculosis* (Mtb-TrxR).[15] Effective inhibition of the validated drug target Mtb-TrxR would allow the development of new drugs for the treatment of tuberculosis, which is still one of the deadliest infectious diseases, with around 1.5 million deaths annually.[21–23] With its substrate thioredoxin (Trx), the TrxR is essential for thiol redox homeostasis and maintaining

infection.[24,25] To date we report the identification of 24 bound fragments as a result of a preliminary analysis of the crystallographic fragment screening.

Results

Library Design

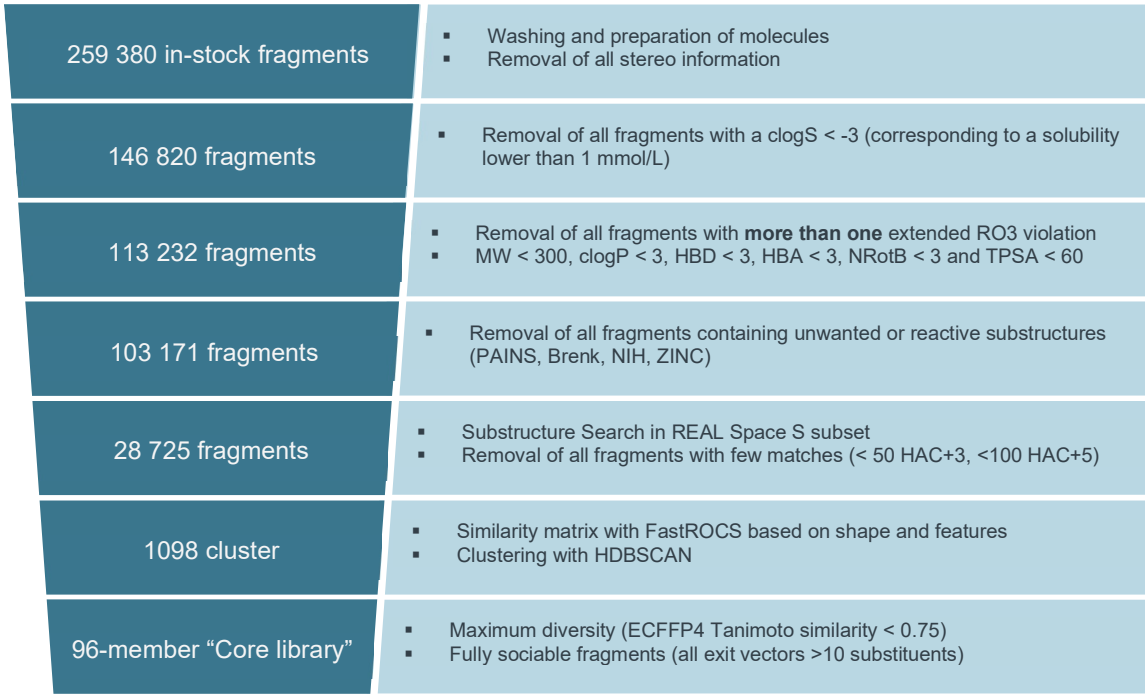

Figure 2: Design workflow of the 96-membered Core library.

The design (Figure 2) is based on Enamine's in-stock fragment library in a process similar to the development of the F2X-Library.[20] As all biophysical screening methods require a certain degree of solubility, the logS based on the dominant protonation state at pH 7.4 was calculated (MOE[26]. A logS of minus three, corresponding to 1 mM/L, was set as the minimum, and all compounds below that threshold were removed. Next, the fragments were analysed regarding their "Rule of Three" compliance. As this rule is the FBDD analogue to Lipinski's famous "Rule of Five", the same guidelines and limitations apply.[27–29] Thereby, the RO3 was taken as an estimate of developability, and all fragments with more than one violation were removed. All fragments not passing the PAINS[30], BRENK[31], NIH[32,33] or ZINC[34] filters were sorted out to prevent artefacts and false positive results during screening and to ease further development. At this point, an estimate of sociability was introduced. Based on the REAL Space S ("simple"), consisting of molecules with high synthesizability, all leadlike compounds (heavy atoms ≤ 25 and logP ≤ 3.5) in it were converted into a substructure-searchable database of roughly 440 million entries. For each fragment, the number of substructure matches in this space was

calculated and based thereon, all with less than 50 matches with up to three more heavy atoms and less than 100 matches with up to five more heavy atoms were removed. To cover the chemical space as efficiently as possible and maximise the diversity of the library, the pairwise similarity for all fragments based on 3D shape and arrangement of chemical features was calculated with OpenEye's FastROCS.[35] Based on the resulting square distance matrix, the hierarchical, density-based clustering algorithm HDBSCAN was used to sort the fragments into clusters with a minimum size of ten.[36] The resulting 1098 clusters contained 76% of the input molecules, whereas 24% were discarded as "noise", not belonging to any cluster. For each cluster, the fragment most similar to all other members was selected as representative. This selection is considered a "General library" suitable for higher throughput screening methods. However, the aim was a 96-membered library suitable for crystallographic screening with two goals: maximise diversity and full sociability.

Therefore, the representative of the largest cluster was taken as the first fragment. Next, the representative from the next largest cluster is added to the selection only if their Tanimoto-similarity based on the FCFP4 fingerprint is below 0.75.[37] Furthermore, an R-group decomposition of their substructure matches in the leadlike subset of the REAL Space S was performed for all fragments. All except one exit vector must have at least ten small (≤ 7 heavy atoms) substituents available to achieve full sociability. This led to a 96-membered "Core library".

Fragment Properties

Fragment libraries must not only represent the available chemical space evenly in terms of structure but also in terms of properties.[28] There is a shift towards smaller and more RO3-compliant fragments for the Core and General libraries.[29] For the Core library, most of the fragments (73%) have a heavy atom count (HAC) between 11-15 and 80% of these fragments have a molecular weight between 140 and 220 Da, thus focusing on the smaller compounds from the in-stock library (Figure 3 A & B). This allows for plenty of room for subsequent optimisation and limits complexity and, possibly, the risk of unfavourable interactions. Three-quarters of the fragments possess one or two hydrogen-bond acceptors, allowing for the formation of strong binding interactions without creating too much complexity (Figure 3 C). Hydrogen-bond donors, however, fell recently under scrutiny, as they can impede bioavailability and solvation and should therefore be limited, especially in the early stage of hit- and lead-development.[38,39] In this regard, 86% of the fragments have only one or zero donors (Figure 3 D). All fragments also show desired medium lipophilicity and polarity, with all logP values below three and only four fragments having a TPSA larger than 60 $Å^2$ (Figure 3 E & F). Also, the focus on solubility during the design stage shifts the distribution of the logS

distinctly towards higher values in contrast to the in-stock library (Figure 3 G). This results in high RO3 compliance as only 11% of the members violate one rule (Figure 3 H).

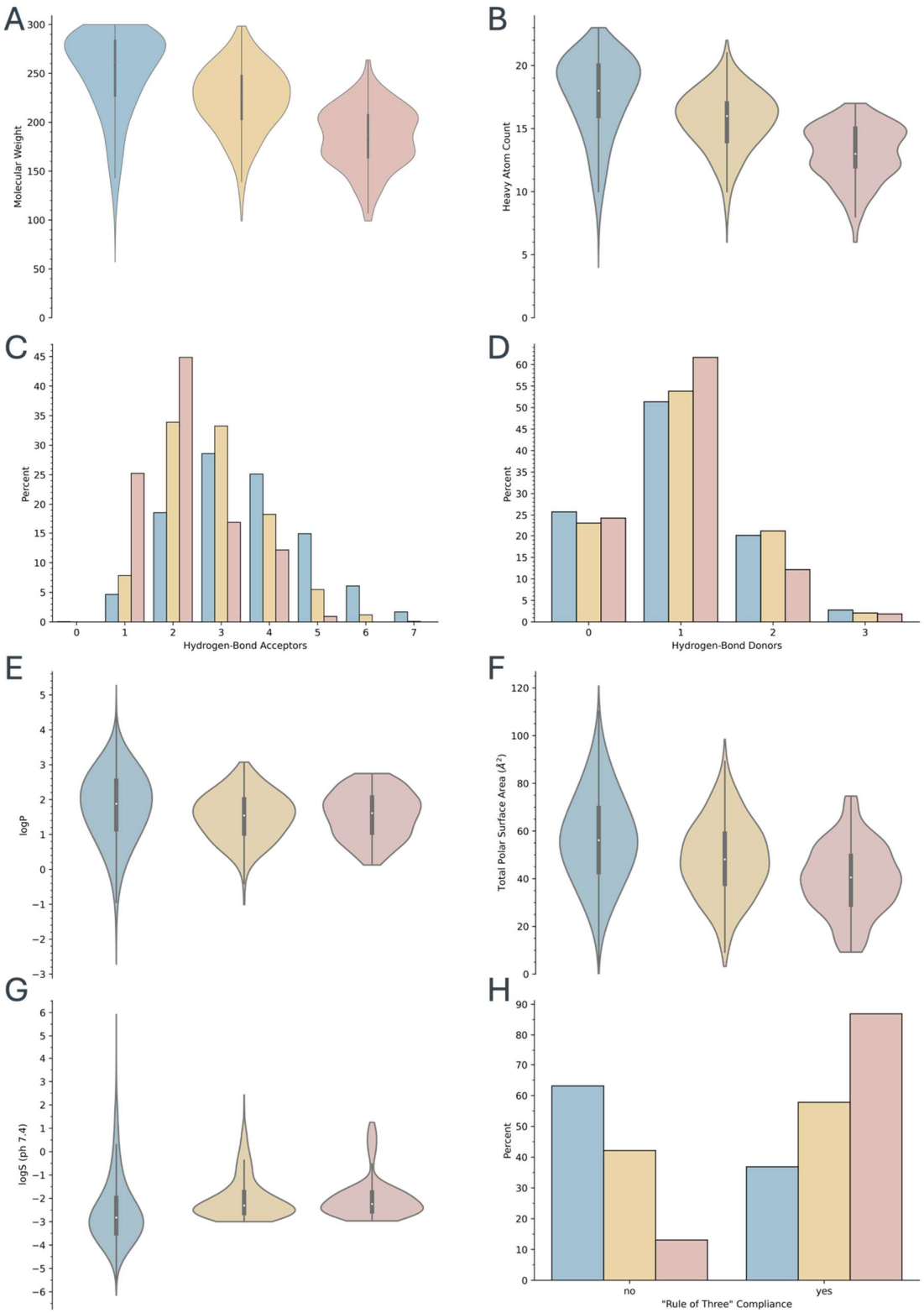

*Figure 3: Physicochemical Properties of the in-stock fragment library (blue), the "General library" (yellow) and the "Core library" (red). **A** Distribution of molecular weight (g/mol) **B** Distribution of non-hydrogen heavy atom count **C** Distribution of hydrogen-bond acceptors **D** Distribution of hydrogen-bond donors **E** Distribution of logP values **F** Distribution of total polar surface area (Å²) **G** Distribution of logS values (calculated for pH 7.4) **H** Distribution of Rule of Three compliance (MW < 300, clogP < 3, HBD < 3, HBA < 3, NRotB < 3 and TPSA < 60).*

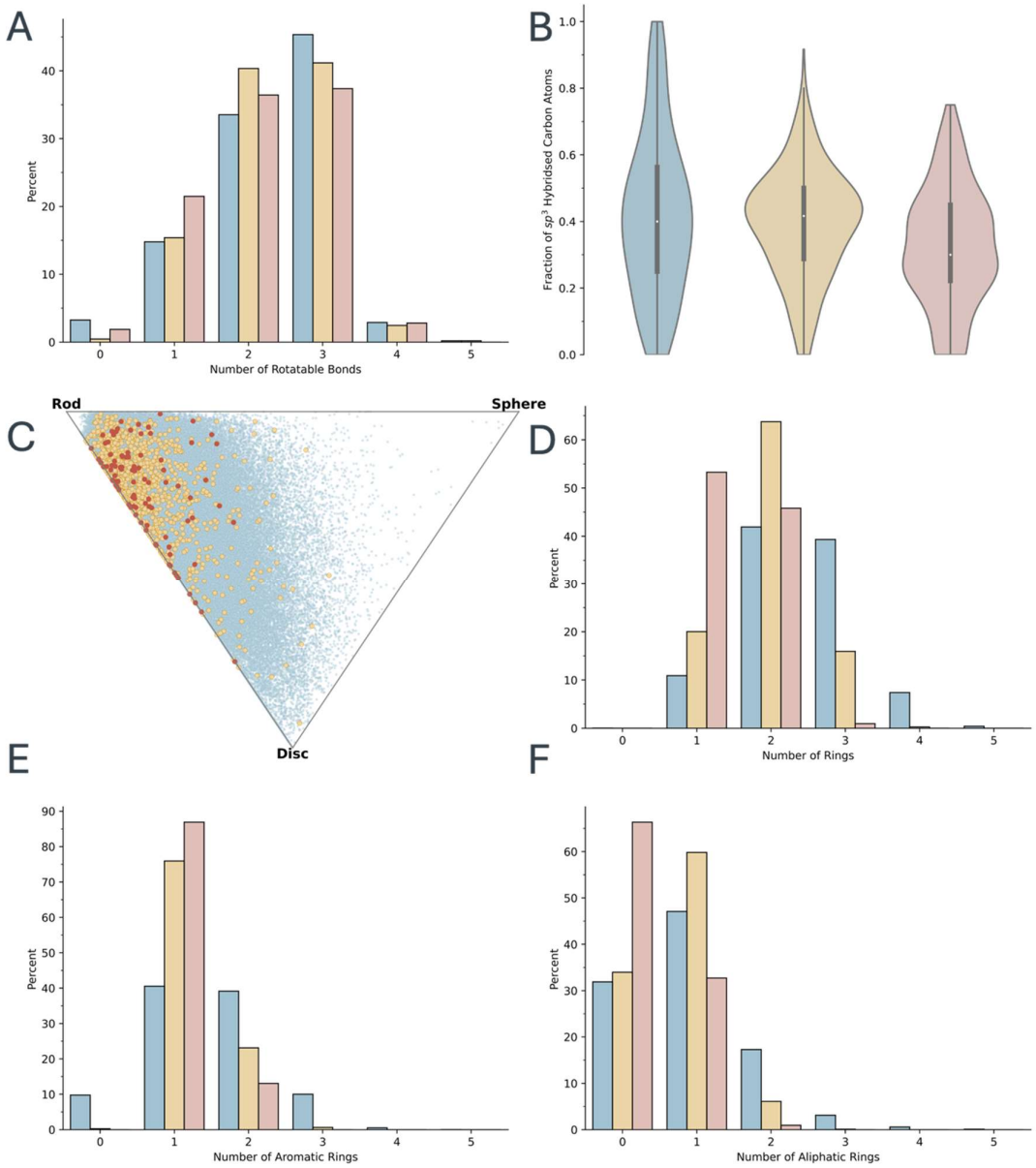

Figure 4: Plots describing 3D-likeness and ring system in the three libraries. In-stock fragment library shown in blue, "General library" in yellow and "Core library" red. ***A*** *Distribution of the number of rotatable bonds* ***B*** *Distribution of the fraction of sp^3-hybridised carbon atoms* ***C*** *Principal moments of inertia (PMI) plot, describing the shape of the molecules in regard to their similarity to a rod, disc and sphere shape* ***D*** *Distribution of the total number of rings* ***E*** *Distribution of the number of aromatic rings* ***F*** *Distribution of the number of aliphatic rings.*

In the past, fragment libraries used to be primarily flat and two-dimensional.[40] Recently, though, there has been a rising attentiveness to escape from this “flatland”.[41–43] Even though using more three-dimensional fragments can result in lower hit rates due to the increased complexity and impede synthetic tractability, a certain degree can also help introduce more diversity and improve the solubility and selectivity of hits.[44–48] In this regard, almost all fragments of the Core Library have at least one rotatable bond and a median fraction of sp^3-hybridised carbon atoms of 32% (Figure 4 A & B). This is also reflected in the principal

moments of inertia plot (Figure 4 C). Almost all of the fragments have some degree of “sphere-likeness”, even though they are close to the “Rod”-“Disc” axis. However, this should be an intuitive observation, as FBDD deals with small and less complex molecules. As rings are ubiquitous in drug design, it is not surprising that all fragments contain at least one ring. Most of the rings being aromatic contributes to the somewhat limited three-dimensionality, primarily due to the focus on sociability (Figure 4 D, E & F).

Additionally, as we aimed for maximum diversity under the constraint of sociability, the library was assembled to cover the available chemical space as best as possible. The average similarity (ECFP4, Tanimoto) of each member to all the others is below 0.4 (Mean 0.31). (Figure 5 A) This implies that the fragments are very dissimilar to each other. Also, regarding the actual coverage of the chemical space, one can see that both the “General” and the “Core” libraries sample the chemical space of the In-Stock fragment library evenly without excessive aggregation in any one area (Figure 5 B).

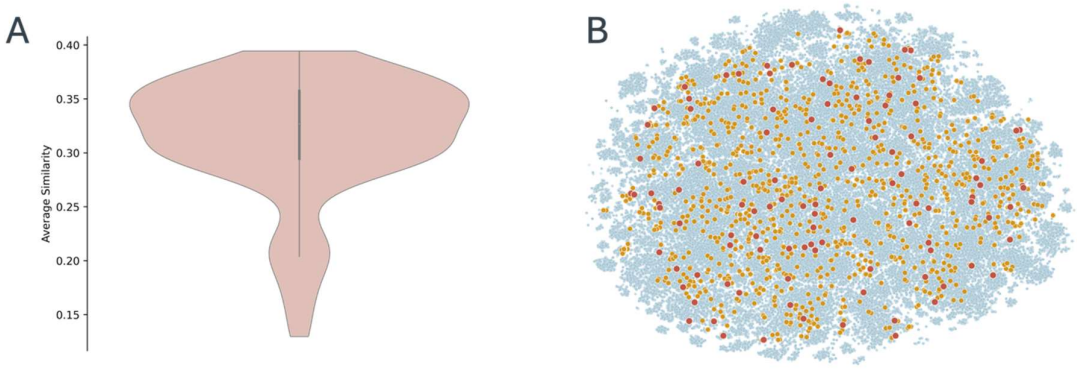

*Figure 5: **A** Distribution of the average similarity of the members of the "Core library" **B** Depiction of the chemical of the three libraries based on t-SNE calculation In-stock fragment library shown in blue, "General library" in yellow and "Core library" red.*

Sociability

The primary aim of this library is full sociability. Therefore, all growth vectors except one must have a minimum of ten small substituents with up to seven heavy atoms. These are the single-point modified derivatives (SPM), which are suitable for exploration of the chemical space directly around the fragment and determination of first-shell structure-activity relationships. (Figure 6). Hundreds to thousands (Median 841) of these SPMs are available for each fragment. Considering the larger leadlike chemical space, derivatives which are substituted in more than one position and with larger substituents, tens to hundreds of thousands (Median 76 532) of possible follow-up compounds become accessible, thus allowing for rapid expansion of binding fragments. As the fragments each belong to a cluster of similar compounds regarding shape and 3D arrangement of chemical features, in addition to growing, the scaffold of a hit can be modified as well.

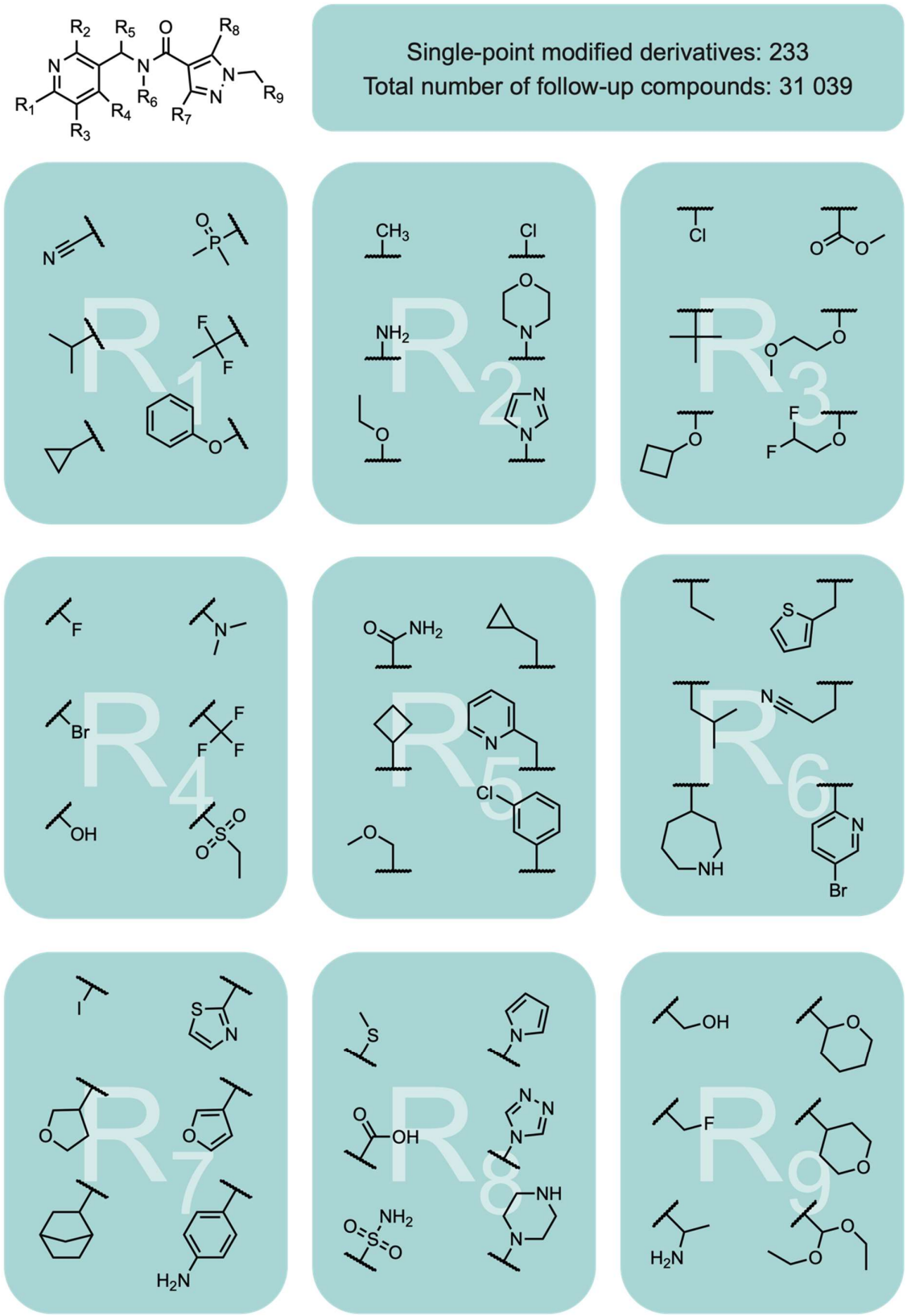

Figure 6: Examples of the substituents available for each growth vector on the example of 1-methyl-N-(pyridin-3-ylmethyl)pyrazole-4-carboxamide. The box in the upper right corner shows the total number of follow up compounds.

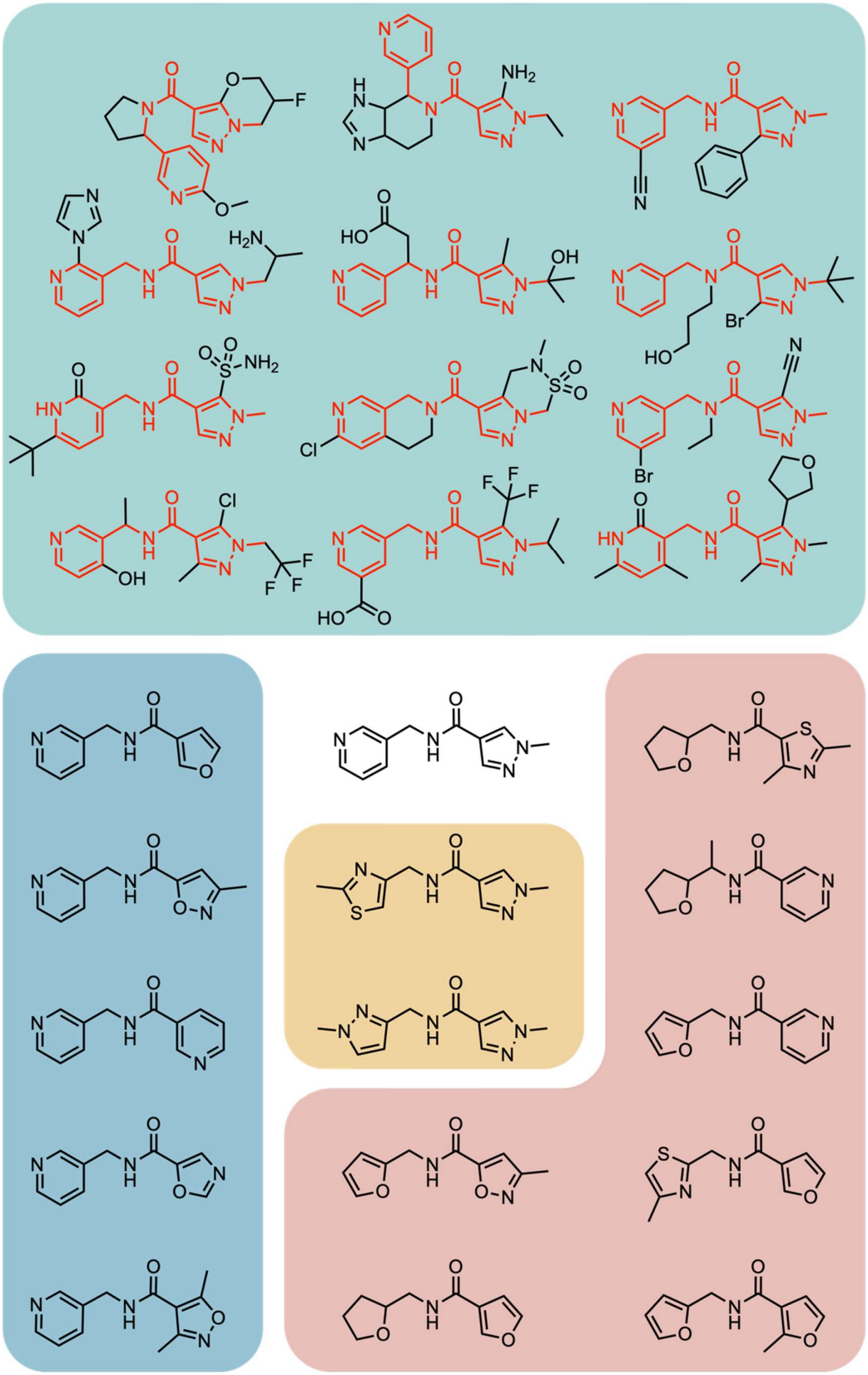

Figure 7: Larger and more substituted follow-up compounds to 1-methyl-N-(pyridin-3-ylmethyl)pyrazole-4-carboxamide (green) with the core scaffold marked in red. Also, various scaffolds are available for each fragment. Modifications of the pyrazole ring (blue), pyridine (yellow), or both ring systems (red) are shown.

Preliminary Fragment Hits

As a test case for our newly designed fragment library, we performed a crystallographic fragment screening with the antibacterial drug target TrxR from *M. smegmatis*. With this protein, a hit rate of 44% was achieved for the F2X entry library.[15] Here, for each fragment, two Msm-TrxR crystals were soaked for 3 hours, flash-frozen and a data set collected at BL14.2 of HZB. The refined data sets obtained from the auto-processing pipelines were screened for bound ligands using *LigandFit*.[49] So far, 24 fragments have been found to bind at eight different sites on the Msm-TrxR (Figure 8). Seven of these fragments are located on the surface (shown in green) and might not influence the function of the enzyme. The remaining 17 fragments are located either in the dimer interaction site (purple), the Trx-binding site (orange) or the NADPH-binding site (cyan).

All three sites are crucial for the enzyme's activity. In general, prokaryotic TrxRs reduce its substrate Trx in a catalytic cascade by an electron transport from the cofactors NADPH to FAD, then to the active disulfide of TrxR and finally to the active dithiol of Trx, so that Trx can then perform its essential function in redox homeostasis.[24,50] In more detail, this process depends on a conformational change between an oxidised (F_O) and a reduced (F_R) conformation of the TrxR. In the F_O conformation, FAD reduces the active disulfide. To allow the reduction of FAD by NADPH and the binding of thioredoxin with subsequent dithiol-disulfide interaction, the NADPH- (Figure 8, grey) and FAD-binding domain (Figure 8, blue) rotate against each other to form the F_R conformation. Also, the active disulfide of the TrxR becomes accessible in the F_R conformation because it is presented on the surface while buried

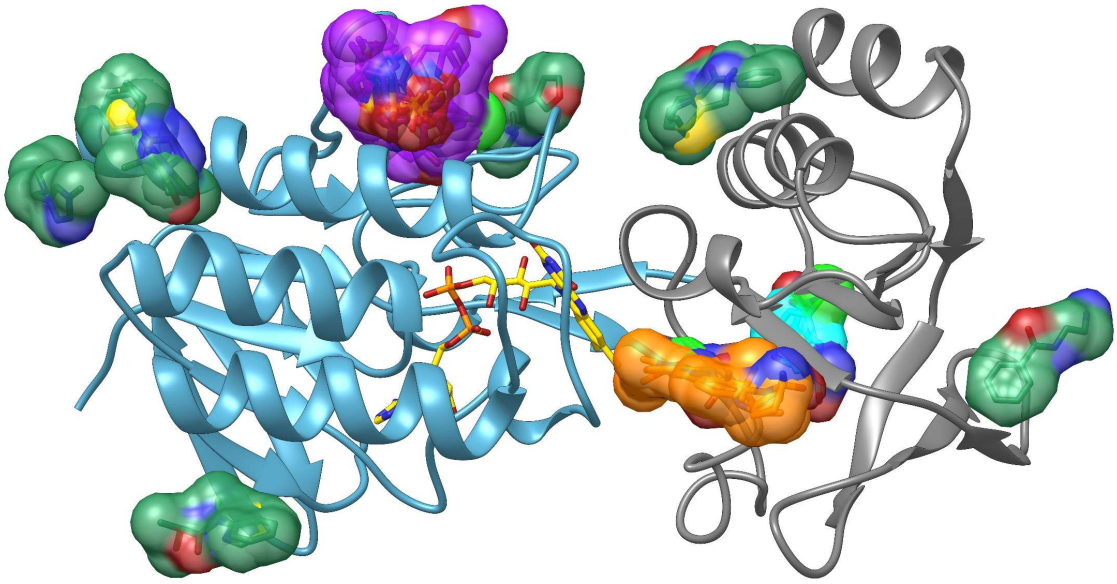

Figure 8: Overview of binding fragments found in the crystallographic fragment screening on Msm-TrxR. 24 fragments were found in eight binding spots located on the surface (green), the dimer interaction site (purple) the Trx-binding site (orange) and the NADPH-binding site (cyan, in the background). The NADPH-binding domain is shown in grey, the FAD-binding domain is shown in blue, and the cofactor FAD is shown in gold.

within the enzyme in the F_O conformation.[50] Suppose this rotation is inhibited due to an arrest in the F_O conformation by a fragment located in the dimer interaction site. In that case, Trx may be unable to bind and interact with the active disulfide. If a fragment binds within the Trx-binding site, Trx binding might also be prevented. In the same manner, if the binding of NADPH is blocked, the enzymatic cascade and thus the activity of the enzyme is prevented.

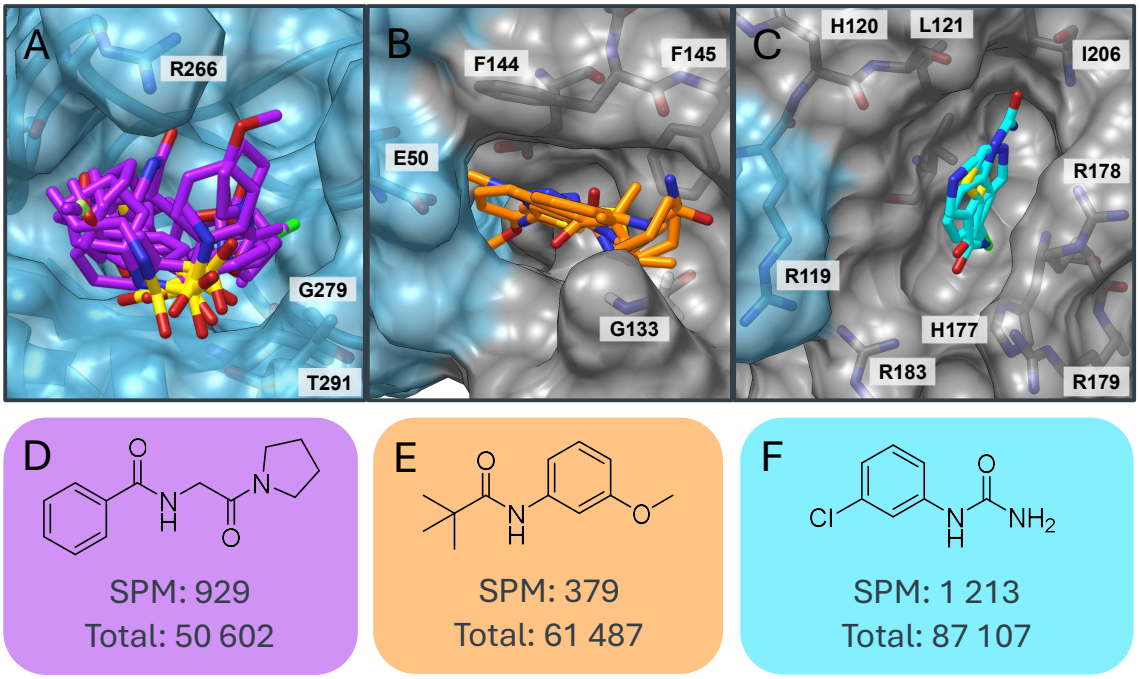

Figure 9: Fragments binding on Msm-TrxR with the FAD-binding domain shown in blue and the NADPH-binding domain shown in grey. Important residues for interactions or the definition of the binding site are highlighted. ***A*** *Eleven fragments bind in the dimer interaction site (purple) in close proximity to Arg266.* ***B*** *Five fragment bind in the Trx-binding site (orange).* ***C*** *Two fragments bind in the NADPH-binding site (cyan).* ***D****,* ***E*** *and* ***F*** *Examples of bound fragments in the dimer- (purple), Trx-binding- (orange) and NADPH-binding site (cyan) with the respective number of single-point modified derivatives (SPM) and the total number of follow-up compounds available.*

Dimer Interaction Site

The dimer interaction site lies within two of the FAD-binding sites of two TrxR protomers and is formed by 60 amino acids, allowing different interaction patterns with potential ligands.[15] Eleven fragments were found that bind to the dimer interaction site (**Fehler! Verweisquelle konnte nicht gefunden werden.** A). The amino acid residues of Arg266, Gly279 and Thr291 play important roles in the formation of the binding site and the latter two are showing hydrogen bonds to two of the bound fragments. Also, all fragments bind symmetrically mirrored in the pocket regarding the other protomer. For clarity, only one binding mode per fragment is shown in **Fehler! Verweisquelle konnte nicht gefunden werden.**. As stated above, the NADPH- and FAD-binding domains must rotate against each other to allow the reaction cascade and binding of Trx. By stabilising the F_O conformation through a ligand in the dimer interaction site which connects the protomers, the functionality of the enzyme might be inhibited. Further

investigation of this binding pocket and the influence of ligand binding on the conformational change are needed.

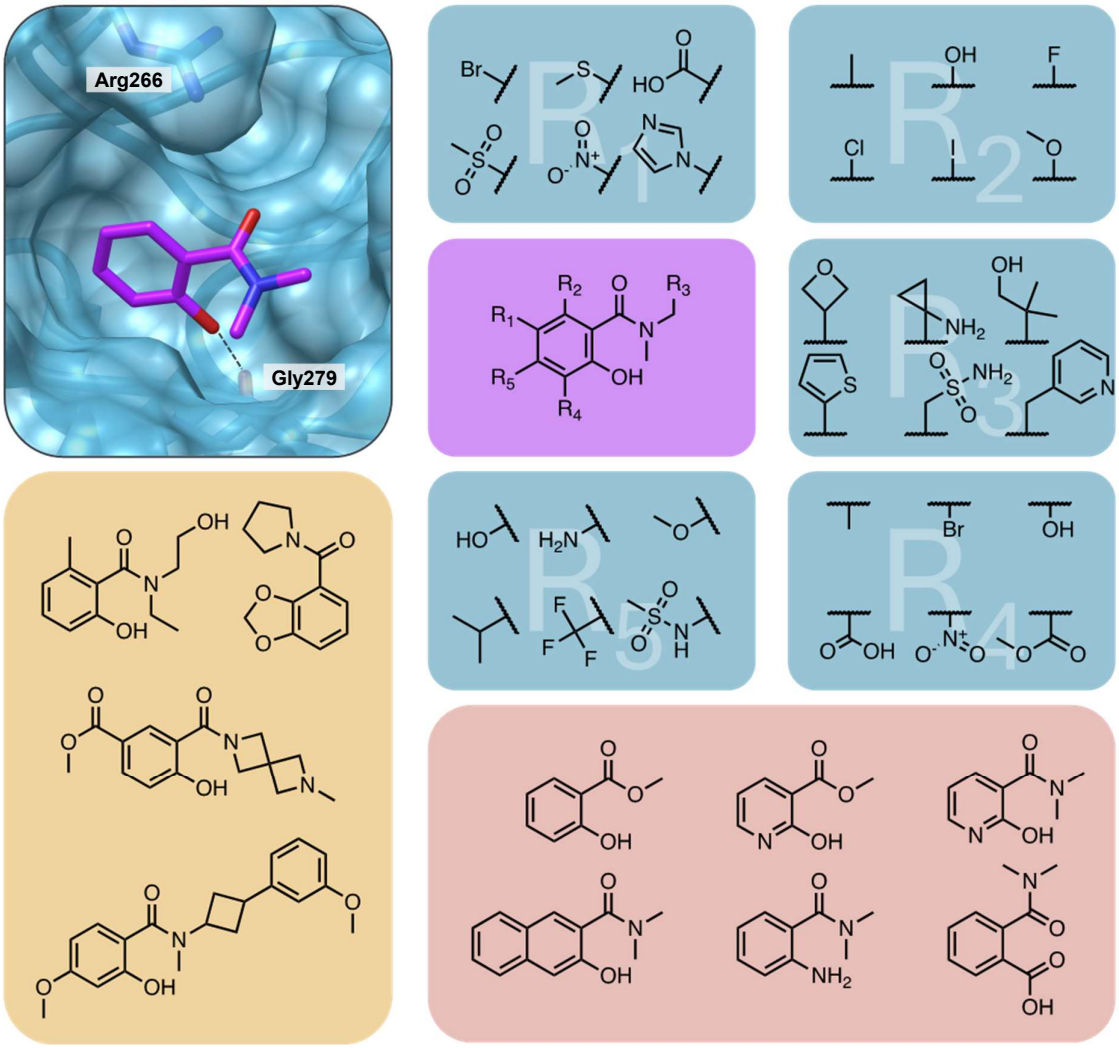

Figure 10: Overview of possible derivatives of one of the hits in the dimer site. The blue boxes exemplify what substituents are available for each growth vector. The hydroxy group would be accessible as well but is necessary for binding in this case. The yellow box shows examples of possible larger and more leadlike follow-up compounds. And in the red box possible scaffold modifications are shown.

Trx-binding Site

The Trx-binding site lies at the interface between the FAD- and NADPH-binding domains. As described above, this binding site is crucial for electron transport and reduction of Trx. In F_R conformation of the reductase, the active disulfide is presented on the surface, thus enabling the dithiol-disulfide interaction after binding of Trx. It was shown previously that an *E. coli* Trx-TrxR complex is formed by the interaction of the Trx-loop Tyr70-Ile75 (Ala67-Ile75 for Msm-TrxR) with a complementary cleft on the respective TrxR.[50,51] Due to high sequence similarity, this can be transferred to Msm-TrxR. Another interaction occurs at *E. coli's* Phe141 and Phe142 (Phe143 and Phe144 for Msm-TrxR) with a hydrophobic pocket described by Lennon

et al.[50] and Koch et al.[23] If fragments bind to these sites, the binding of Trx might be inhibited. Since the bound fragments shown in **Fehler! Verweisquelle konnte nicht gefunden werden.** B are located in the complementary cleft to the Trx-loop Ala67-Ile75 next to TrxR's Glu50, Thr234 and Phe144, the insertion of the loop could get sterically hindered, and thus, the formation of a Trx-TrxR complex should be prevented (**Fehler! Verweisquelle konnte nicht gefunden werden.** B).

NADPH-binding Site

The enzymatic activity of the TrxR is highly dependent on the binding of the cofactor NADPH as it provides reducing equivalents for the reduction of FAD within the catalytic cascade, as described above. Two fragments were observed to bind in the NADPH-binding site (Figure 9 C). One of these fragments has formed an H-bond with His177. Other important amino acids include Arg119, His120, Leu121, Arg178, Arg179, Arg183, and Ile206. In a previous fragment screening on the same protein, H-bonds could be identified to several of the amino acids mentioned above, while others play a role in forming the binding pocket. Since NADPH is a widespread cofactor for many enzymes, an inhibitor for this mycobacterial NADPH-binding pocket would have to be very selective. Therefore, a more detailed evaluation of the hits and their binding is necessary and will be performed after a full evaluation of the fragment screening.

Methods

Library Design

Preparation of the database was performed using MOE (2022.2).[26] Washing, desalting, neutralising charges, and calculating the dominant protonation state were done using the built-in functions. Filtering unwanted substructures was performed with RDKit's Filter catalogue module using the PAINS, BRENK, NIH, and ZINC parameters.[52] Enamine kindly provided the REAL Space S subset in annotated files. All molecules with a logP lower or equal to 3.5 and less than 26 heavy atoms (442 000 626 compounds) were transformed into a substructure-searchable database with OpenEye's OEChem toolkit, optimised for using SMARTS as queries.[53] All putative fragments' number of substructure matches and the respective heavy atom counts were calculated by querying the databases using the OEChem toolkit again.

The pairwise similarity was calculated using OpenEye's FastROCS. Ten conformers per molecule were calculated using OpenEye's OMEGA tool with the "strict" flag set to false.[54] These were used as input for calculating the square distance matrix using FastROCS and the provided Python script ("ShapeDistanceMatrix.py").[35] This matrix was transformed into an

array and clustered using HDBSCAN (metric = “precomputed”, min_cluster_size = 10, cluster_selection_method = “leaf”).[36] The representative for each cluster was calculated using the previously calculated FastROCS similarities.

The possible growth vectors were enumerated for all remaining fragments, and the substructure-searchable databases were queried for molecules substituted at only one of the respective growth vectors with up to seven more heavy atoms. The matches were then decomposed into their substituents using RDKit’s RGroupDecomposition module.

Protein Expression and Purification

Expression and purification were done as already described by Füsser et al. with slight modifications.[15] The vector encoding for *M. smegmatis* TrxR (pCDF6P) contains an *N*-terminal GST-His-tag for the protein and was heterogeneously overexpressed in *E. coli* BL21 (DE3) cells. The cells were cultivated in TB-medium with 50 µg mL^{-1} streptomycin at 37 °C. After reaching an OD_{600} of 0.6, the culture was cooled on ice for 30 minutes. The protein expression was induced by adding 1 mM IPTG and continued for 18 hours at 16 °C and 170 rpm. The cells were harvested (2,981 x*g*, 15 minutes, 4 °C) and stored at -20 °C until usage.

Cell pellets were resuspended in GST buffer (50 mM Tris/HCl, 300 mM NaCl, 2 mM fresh DTT, pH 7.5) and pressed through a 1000 µL pipette tip. The suspension was mixed with 2.5 µg mL^{-1} DNase I, 100 µg mL^{-1} lysozyme and 1x protease inhibitor mix (SERVA, Heidelberg) and incubated for 30 minutes at 4 °C. The cell lysis was carried out using an LM20 Microfluidizer™ at 20,000 psi and centrifugation (17,000 x*g*, 30 minutes, 4 °C). The supernatant was transferred on a 2 mL glutathione agarose resin (SERVA, Heidelberg) twice, washed three times with 5 mL GST buffer and incubated for 18 hours at 4 °C with 2.87 mg mL^{-1} PreScission protease (provided by Bianca Berkenfeld) in 2 mL GST buffer. The protein was eluted with 4 mL GST buffer. The eluate was incubated with a spatula tip of FAD solved in 1 mL GST buffer for 1 hour at 4 °C. The protein solution was concentrated (2,981 x*g*, 10 minutes, 4 °C) and washed with GST buffer using the Amicon® Pro Purification System (Merck Millipore) with a 10 kDa cut-off. The protein solution was stored at -80 °C until usage.

As a second purification step, a size exclusion chromatography was performed on an Enrich™ SEC650 column on a Bio-Rad NGC™ chromatography system (Hercules, USA) using the gel filtration buffer (10 mM Tris/HCl, pH 8.0). Fractions containing the protein were combined and concentrated using the Amicon® Pro Purification System with a 10 kDa cut-off.

Crystallisation

M. smegmatis TrxR (23 mg mL^{-1} in gel filtration buffer) was mixed with 10 mM DTT, incubated for 1 hour at 4 °C and centrifuged (21,910 x*g*, 10 minutes, 4 °C). Crystals were grown by

mixing 1 µL of the protein solution with 1 µL crystallisation buffer (2.16 M sodium malonate, 10 % (*v*/*v*) glycerol, pH 6.5) and incubating at 20 °C for 8 and 13 days on MRC maxi plate – PS (Jena Bioscience, DE) and MRC 2 well crystallisation plate – PS (Jena Bioscience, DE).

Soaking

For each fragment, 2 wells of an MRC 3 well crystallisation plate – PS (Jena Bioscience, DE) were prepared with a nominal amount of 100 mM fragment in 0.4 µL and dried at 40 °C for 18 hours. 0.4 µL soaking solution (2.05 M sodium malonate, 9.5 % (*v*/*v*) glycerol, 5 % (*v*/*v*) DMSO, pH 6.5) was added and incubated at RT for 5 minutes. Crystals were soaked by transferring at least three crystals into each drop and incubating for 3 hours at 20 °C. Two crystals per condition were picked and flash-frozen in liquid nitrogen. An additional number of 24 crystals were soaked in the soaking solution without presence of a fragment for data collection of the apo structures for subsequent analysis using PanDDA.[55]

Data Collection

Data collection was carried out at the beamline MX-14.2 at the BESSY II synchrotron radiation source operated by Helmholtz-Zentrum Berlin.[56] Diffraction data was collected at 100 K using a PILATUS detector. For each data set, 1,200 images with an oscillation range of 0.1° and an exposure time of 0.15 s were recorded at full transmission. In total, 210 data sets were collected.

Data Processing and Hit Identification

Collected data sets were processed using XDSAPP.[57] Crystals belonged to space group $P3_121$ and showed a mean resolution of 1.99 Å. The data was further processed using the automated refinement pipelines fspipeline and DIMPLE with PDB model 8CCI as input.[58–60] Preliminary hit identification was carried out using LigandFit.[49]

Conclusion

The rapid rise of ultra-large virtual chemical libraries enlarges the easily accessible chemical space massively. This, in turn, allows the design of fragment libraries not only with diversity in mind but with a “sociability-first” approach. Even by using only a fraction of the larger REAL Space, there is a multitude of fragments that show full sociability. While maintaining a high degree of diversity, we constructed a library of fragments that can be grown in virtually all directions with small and large substituents alike and can have their scaffolds easily modified. This allows for almost immediate follow-up to any interesting screening hits, thus shortening

the hit-to-lead time massively. Fragments only substituted in one position allow for quick first-shell SAR and improvement of the efficiency of the fragment itself, whereas the larger and more complex compounds allow for growing in the desired directions and improvement of physicochemical parameters. Additionally, the properties of the library are well inside the desired ranges, minimising constraints during development.

For the test case of finding inhibitors for a mycobacterial TrxR as antituberculotic agents, several binding fragments could be identified. Due to the design of our social library, direct follow-up compounds are available for the hits. In total, 1.3 million follow-ups are available for the 17 fragments located in the three relevant binding pockets described above. This means that, on average, roughly 77 thousand follow-ups are available for each of the fragments for expansion. In combination with structure-based design methods like docking, promising fragment extensions are now very fast accessible.

With this small and efficient library at hand, showing the promise of the “sociability-first” concept, we will transfer it to various other libraries. Using the entire REAL Space allows for even more diverse fragments and follow-up compounds and the design of more extensive libraries suitable for higher-throughput methods. Furthermore, this concept can be easily applied to libraries specialising on different concepts and screening techniques (covalent binders, natural product-likeness, high sp^3-fraction, minifrags or ^{19}F fragments). Fluorinated and covalently modified analogues are readily available from Enamine’s in-stock screening collection.

Acknowledgements

The financial support by the German Research Foundation (DFG) in the context of the Heisenberg-Program and by the German Center for Infection Research (DZIF; Project TTU 02.906) is gratefully acknowledged. Measurements were carried out at Beamline 14.2 at the BESSY II electron storage ring operated by the Helmholtz-Zentrum Berlin für Materialien und Energie.[13] We would like to thank Tom Crosskey and Frank Lennartz for their assistance during the experiment.

Bibliography

(1) Murray, C. W.; Rees, D. C. The Rise of Fragment-Based Drug Discovery. *Nat. Chem.* **2009**, *1* (3), 187–192. https://doi.org/10.1038/nchem.217.

(2) Benner, B.; Good, L.; Quiroga, D.; Schultz, T. E.; Kassem, M.; Carson, W. E.; Cherian, M. A.; Sardesai, S.; Wesolowski, R. Pexidartinib, a Novel Small Molecule CSF-1R Inhibitor in Use for Tenosynovial Giant Cell Tumor: A Systematic Review of Pre-Clinical and Clinical Development. *Drug Des. Devel. Ther.* **2020**, *14*, 1693–1704. https://doi.org/10.2147/DDDT.S253232.

(3) Kim, A.; Cohen, M. S. The Discovery of Vemurafenib for the Treatment of BRAF-Mutated Metastatic Melanoma. *Expert Opin. Drug Discov.* **2016**, *11* (9), 907–916. https://doi.org/10.1080/17460441.2016.1201057.

(4) W. Murray, C.; R. Newell, D.; Angibaud, P. A Successful Collaboration between Academia, Biotech and Pharma Led to Discovery of Erdafitinib, a Selective FGFR Inhibitor Recently Approved by the FDA. *MedChemComm* **2019**, *10* (9), 1509–1511. https://doi.org/10.1039/C9MD90044F.

(5) Fairbrother, W. J.; Leverson, J. D.; Sampath, D.; Souers, A. J. Discovery and Development of Venetoclax, a Selective Antagonist of BCL-2. In *Successful Drug Discovery*; John Wiley & Sons, Ltd, 2019; pp 225–245. https://doi.org/10.1002/9783527814695.ch9.

(6) Lanman, B. A.; Allen, J. R.; Allen, J. G.; Amegadzie, A. K.; Ashton, K. S.; Booker, S. K.; Chen, J. J.; Chen, N.; Frohn, M. J.; Goodman, G.; Kopecky, D. J.; Liu, L.; Lopez, P.; Low, J. D.; Ma, V.; Minatti, A. E.; Nguyen, T. T.; Nishimura, N.; Pickrell, A. J.; Reed, A. B.; Shin, Y.; Siegmund, A. C.; Tamayo, N. A.; Tegley, C. M.; Walton, M. C.; Wang, H.-L.; Wurz, R. P.; Xue, M.; Yang, K. C.; Achanta, P.; Bartberger, M. D.; Canon, J.; Hollis, L. S.; McCarter, J. D.; Mohr, C.; Rex, K.; Saiki, A. Y.; San Miguel, T.; Volak, L. P.; Wang, K. H.; Whittington, D. A.; Zech, S. G.; Lipford, J. R.; Cee, V. J. Discovery of a Covalent Inhibitor of KRASG12C (AMG 510) for the Treatment of Solid Tumors. *J. Med. Chem.* **2020**, *63* (1), 52–65. https://doi.org/10.1021/acs.jmedchem.9b01180.

(7) Schoepfer, J.; Jahnke, W.; Berellini, G.; Buonamici, S.; Cotesta, S.; Cowan-Jacob, S. W.; Dodd, S.; Drueckes, P.; Fabbro, D.; Gabriel, T.; Groell, J.-M.; Grotzfeld, R. M.; Hassan, A. Q.; Henry, C.; Iyer, V.; Jones, D.; Lombardo, F.; Loo, A.; Manley, P. W.; Pellé, X.; Rummel, G.; Salem, B.; Warmuth, M.; Wylie, A. A.; Zoller, T.; Marzinzik, A. L.; Furet, P. Discovery of Asciminib (ABL001), an Allosteric Inhibitor of the Tyrosine Kinase Activity of BCR-ABL1. *J. Med. Chem.* **2018**, *61* (18), 8120–8135. https://doi.org/10.1021/acs.jmedchem.8b01040.

(8) Turner, N. C.; Oliveira, M.; Howell, S. J.; Dalenc, F.; Cortes, J.; Gomez Moreno, H. L.; Hu, X.; Jhaveri, K.; Krivorotko, P.; Loibl, S.; Morales Murillo, S.; Okera, M.; Park, Y. H.; Sohn, J.; Toi, M.; Tokunaga, E.; Yousef, S.; Zhukova, L.; de Bruin, E. C.; Grinsted, L.; Schiavon, G.; Foxley, A.; Rugo, H. S.; CAPItello-291 Study Group. Capivasertib in Hormone Receptor-Positive Advanced Breast Cancer. *N. Engl. J. Med.* **2023**, *388* (22), 2058–2070. https://doi.org/10.1056/NEJMoa2214131.

(9) Erlanson, D. *Practical Fragments: Fragments in the clinic: 2024 edition*. Practical Fragments. http://practicalfragments.blogspot.com/2024/02/fragments-in-clinic-2024-edition.html (accessed 2024-05-08).

(10) Hall, R. J.; Mortenson, P. N.; Murray, C. W. Efficient Exploration of Chemical Space by Fragment-Based Screening. *Prog. Biophys. Mol. Biol.* **2014**, *116* (2–3), 82–91. https://doi.org/10.1016/j.pbiomolbio.2014.09.007.

(11) Doak, B. C.; Norton, R. S.; Scanlon, M. J. The Ways and Means of Fragment-Based Drug Design. *Pharmacol. Ther.* **2016**, *167*, 28–37. https://doi.org/10.1016/j.pharmthera.2016.07.003.

(12) Revillo Imbernon, J.; Jacquemard, C.; Bret, G.; Marcou, G.; Kellenberger, E. Comprehensive Analysis of Commercial Fragment Libraries. *RSC Med. Chem.* **2022**, *13* (3), 300–310. https://doi.org/10.1039/D1MD00363A.
(13) St. Denis, J. D.; Hall, R. J.; Murray, C. W.; Heightman, T. D.; Rees, D. C. Fragment-Based Drug Discovery: Opportunities for Organic Synthesis. *RSC Med. Chem.* **2021**, *12* (3), 321–329. https://doi.org/10.1039/D0MD00375A.
(14) Erlanson, D. *Practical Fragments: Poll results: synthetic challenges are pervasive in FBLD*. Practical Fragments. http://practicalfragments.blogspot.com/2021/07/poll-results-synthetic-challenges-are.html (accessed 2024-03-24).
(15) Füsser, F. T.; Wollenhaupt, J.; Weiss, M. S.; Kümmel, D.; Koch, O. Novel Starting Points for Fragment-Based Drug Design against Mycobacterial Thioredoxin Reductase Identified Using Crystallographic Fragment Screening. *Acta Crystallogr. Sect. Struct. Biol.* **2023**, *79* (9), 857–865. https://doi.org/10.1107/S2059798323005223.
(16) Janssen, Philipp. Fragment-Based Inhibitor Design Based on an Unsociable Fragment. Master's Thesis, University of Münster, Münster, 2022.
(17) Cox, O. B.; Krojer, T.; Collins, P.; Monteiro, O.; Talon, R.; Bradley, A.; Fedorov, O.; Amin, J.; Marsden, B. D.; Spencer, J.; Von Delft, F.; Brennan, P. E. A Poised Fragment Library Enables Rapid Synthetic Expansion Yielding the First Reported Inhibitors of PHIP(2), an Atypical Bromodomain. *Chem. Sci.* **2016**, *7* (3), 2322–2330. https://doi.org/10.1039/C5SC03115J.
(18) Sreeramulu, S.; Richter, C.; Kuehn, T.; Azzaoui, K.; Blommers, M. J. J.; Del Conte, R.; Fragai, M.; Trieloff, N.; Schmieder, P.; Nazaré, M.; Specker, E.; Ivanov, V.; Oschkinat, H.; Banci, L.; Schwalbe, H. NMR Quality Control of Fragment Libraries for Screening. *J. Biomol. NMR* **2020**, *74* (10–11), 555–563. https://doi.org/10.1007/s10858-020-00327-9.
(19) *REAL Fragment Library | Chemspace*. https://chem-space.com/compounds/real-fragment_library?utm_medium=linkedin&utm_term=REAL_Fragment_Library (accessed 2024-04-22).
(20) Wollenhaupt, J.; Metz, A.; Barthel, T.; Lima, G. M. A.; Heine, A.; Mueller, U.; Klebe, G.; Weiss, M. S. F2X-Universal and F2X-Entry: Structurally Diverse Compound Libraries for Crystallographic Fragment Screening. *Structure* **2020**, *28* (6), 694-706.e5. https://doi.org/10.1016/j.str.2020.04.019.
(21) Koch, O.; Bering, L. *MYOBACTERIUM TUBERCULOSIS*-THIOREDOXIN REDUCTASE INHIBITOR AS AN ANTITUBERCULAR AGENT, January 10, 2019. https://patentscope.wipo.int/search/en/detail.jsf?docId=WO2019007710 (accessed 2024-03-13).
(22) World Health Organization. *Global Tuberculosis Report 2021*; World Health Organization: Geneva, 2021.
(23) Koch, O.; Jäger, T.; Heller, K.; Khandavalli, P. C.; Pretzel, J.; Becker, K.; Flohé, L.; Selzer, P. M. Identification of *M. Tuberculosis* Thioredoxin Reductase Inhibitors Based on High-Throughput Docking Using Constraints. *J. Med. Chem.* **2013**, *56* (12), 4849–4859. https://doi.org/10.1021/jm3015734.
(24) Lu, J.; Vlamis-Gardikas, A.; Kandasamy, K.; Zhao, R.; Gustafsson, T. N.; Engstrand, L.; Hoffner, S.; Engman, L.; Holmgren, A. Inhibition of Bacterial Thioredoxin Reductase: An Antibiotic Mechanism Targeting Bacteria Lacking Glutathione. *FASEB J.* **2013**, *27* (4), 1394–1403. https://doi.org/10.1096/fj.12-223305.
(25) Lin, K.; O'Brien, K. M.; Trujillo, C.; Wang, R.; Wallach, J. B.; Schnappinger, D.; Ehrt, S. Mycobacterium Tuberculosis Thioredoxin Reductase Is Essential for Thiol Redox Homeostasis but Plays a Minor Role in Antioxidant Defense. *PLOS Pathog.* **2016**, *12* (6), e1005675. https://doi.org/10.1371/journal.ppat.1005675.
(26) Molecular Operating Environment (MOE), 2022.02 Chemical Computing Group ULC, 910-1010 Sherbrooke St. W., Montreal, QC H3A 2R7, 2024.
(27) Lipinski, C. A.; Lombardo, F.; Dominy, B. W.; Feeney, P. J. Experimental and Computational Approaches to Estimate Solubility and Permeability in Drug Discovery and Development Settings. *Adv. Drug Deliv. Rev.* **2001**, *46* (1–3), 3–26. https://doi.org/10.1016/s0169-409x(00)00129-0.

(28) Keserű, G. M.; Erlanson, D. A.; Ferenczy, G. G.; Hann, M. M.; Murray, C. W.; Pickett, S. D. Design Principles for Fragment Libraries: Maximizing the Value of Learnings from Pharma Fragment-Based Drug Discovery (FBDD) Programs for Use in Academia. *J. Med. Chem.* **2016**, *59* (18), 8189–8206. https://doi.org/10.1021/acs.jmedchem.6b00197.
(29) Jhoti, H.; Williams, G.; Rees, D. C.; Murray, C. W. The “rule of Three” for Fragment-Based Drug Discovery: Where Are We Now? *Nat. Rev. Drug Discov.* **2013**, *12* (8), 644–644. https://doi.org/10.1038/nrd3926-c1.
(30) Baell, J. B.; Holloway, G. A. New Substructure Filters for Removal of Pan Assay Interference Compounds (PAINS) from Screening Libraries and for Their Exclusion in Bioassays. *J. Med. Chem.* **2010**, *53* (7), 2719–2740. https://doi.org/10.1021/jm901137j.
(31) Brenk, R.; Schipani, A.; James, D.; Krasowski, A.; Gilbert, I. H.; Frearson, J.; Wyatt, P. G. Lessons Learnt from Assembling Screening Libraries for Drug Discovery for Neglected Diseases. *ChemMedChem* **2008**, *3* (3), 435–444. https://doi.org/10.1002/cmdc.200700139.
(32) Doveston, R. G.; Tosatti, P.; Dow, M.; Foley, D. J.; Li, H. Y.; Campbell, A. J.; House, D.; Churcher, I.; Marsden, S. P.; Nelson, A. A Unified Lead-Oriented Synthesis of over Fifty Molecular Scaffolds. *Org. Biomol. Chem.* **2015**, *13* (3), 859–865. https://doi.org/10.1039/C4OB02287D.
(33) Jadhav, A.; Ferreira, R. S.; Klumpp, C.; Mott, B. T.; Austin, C. P.; Inglese, J.; Thomas, C. J.; Maloney, D. J.; Shoichet, B. K.; Simeonov, A. Quantitative Analyses of Aggregation, Autofluorescence, and Reactivity Artifacts in a Screen for Inhibitors of a Thiol Protease. *J. Med. Chem.* **2010**, *53* (1), 37–51. https://doi.org/10.1021/jm901070c.
(34) Irwin, J. J.; Shoichet, B. K. ZINC − A Free Database of Commercially Available Compounds for Virtual Screening. *J. Chem. Inf. Model.* **2005**, *45* (1), 177–182. https://doi.org/10.1021/ci049714+.
(35) FastROCS TK 2.2.2. OpenEye, Cadence Molecular Sciences, Santa Fe, NM. Http://Www.Eyesopen.Com.
(36) McInnes, L.; Healy, J.; Astels, S. Hdbscan: Hierarchical Density Based Clustering. *J. Open Source Softw.* **2017**, *2* (11), 205. https://doi.org/10.21105/joss.00205.
(37) Rogers, D.; Hahn, M. Extended-Connectivity Fingerprints. *J. Chem. Inf. Model.* **2010**, *50* (5), 742–754. https://doi.org/10.1021/ci100050t.
(38) Kenny, P. Hydrogen Bond Donors in Drug Design. June 28, 2022. https://doi.org/10.26434/chemrxiv-2022-0mzxq.
(39) Baell, J.; Congreve, M.; Leeson, P.; Abad-Zapatero, C. Ask the Experts: Past, Present and Future of the Rule of Five. *Future Med. Chem.* **2013**, *5* (7), 745–752. https://doi.org/10.4155/fmc.13.61.
(40) Morley, A. D.; Pugliese, A.; Birchall, K.; Bower, J.; Brennan, P.; Brown, N.; Chapman, T.; Drysdale, M.; Gilbert, I. H.; Hoelder, S.; Jordan, A.; Ley, S. V.; Merritt, A.; Miller, D.; Swarbrick, M. E.; Wyatt, P. G. Fragment-Based Hit Identification: Thinking in 3D. *Drug Discov. Today* **2013**, *18* (23), 1221–1227. https://doi.org/10.1016/j.drudis.2013.07.011.
(41) Kidd, S. L.; Osberger, T. J.; Mateu, N.; Sore, H. F.; Spring, D. R. Recent Applications of Diversity-Oriented Synthesis Toward Novel, 3-Dimensional Fragment Collections. *Front. Chem.* **2018**, *6*, 460. https://doi.org/10.3389/fchem.2018.00460.
(42) Klein, H. F.; Hamilton, D. J.; de Esch, I. J. P.; Wijtmans, M.; O’Brien, P. Escape from Planarity in Fragment-Based Drug Discovery: A Synthetic Strategy Analysis of Synthetic 3D Fragment Libraries. *Drug Discov. Today* **2022**, *27* (9), 2484–2496. https://doi.org/10.1016/j.drudis.2022.05.021.
(43) Lovering, F.; Bikker, J.; Humblet, C. Escape from Flatland: Increasing Saturation as an Approach to Improving Clinical Success. *J. Med. Chem.* **2009**, *52* (21), 6752–6756. https://doi.org/10.1021/jm901241e.
(44) Hann, M. M.; Leach, A. R.; Harper, G. Molecular Complexity and Its Impact on the Probability of Finding Leads for Drug Discovery. *J. Chem. Inf. Comput. Sci.* **2001**, *41* (3), 856–864. https://doi.org/10.1021/ci000403i.

(45) Caplin, M. J.; Foley, D. J. Emergent Synthetic Methods for the Modular Advancement of Sp ^{3} -Rich Fragments. *Chem. Sci.* **2021**, *12* (13), 4646–4660. https://doi.org/10.1039/D1SC00161B.
(46) Fuller, N.; Spadola, L.; Cowen, S.; Patel, J.; Schönherr, H.; Cao, Q.; McKenzie, A.; Edfeldt, F.; Rabow, A.; Goodnow, R. An Improved Model for Fragment-Based Lead Generation at AstraZeneca. *Drug Discov. Today* **2016**, *21* (8), 1272–1283. https://doi.org/10.1016/j.drudis.2016.04.023.
(47) Yan, A.; Gasteiger, J. Prediction of Aqueous Solubility of Organic Compounds Based on a 3D Structure Representation. *J. Chem. Inf. Comput. Sci.* **2003**, *43* (2), 429–434. https://doi.org/10.1021/ci025590u.
(48) Johnson, J. A.; Nicolaou, C. A.; Kirberger, S. E.; Pandey, A. K.; Hu, H.; Pomerantz, W. C. K. Evaluating the Advantages of Using 3D-Enriched Fragments for Targeting BET Bromodomains. *ACS Med. Chem. Lett.* **2019**, *10* (12), 1648–1654. https://doi.org/10.1021/acsmedchemlett.9b00414.
(49) Terwilliger, T. C.; Klei, H.; Adams, P. D.; Moriarty, N. W.; Cohn, J. D. Automated Ligand Fitting by Core-Fragment Fitting and Extension into Density. *Acta Crystallogr. D Biol. Crystallogr.* **2006**, *62* (8), 915–922. https://doi.org/10.1107/S0907444906017161.
(50) Lennon, B. W.; Williams, C. H.; Ludwig, M. L. Twists in Catalysis: Alternating Conformations of *Escherichia Coli* Thioredoxin Reductase. *Science* **2000**, *289* (5482), 1190–1194. https://doi.org/10.1126/science.289.5482.1190.
(51) Lennon, B. W.; Williams, C. H.; Ludwig, M. L. Crystal Structure of a Complex Between Thioredoxin Reductase, Thioredoxin, and the NADP+ Analog, AADP+, 2000. https://doi.org/10.2210/pdb1f6m/pdb.
(52) Landrum, G.; Tosco, P.; Kelley, B.; Ric; Cosgrove, D.; Sriniker; Gedeck; Vianello, R.; NadineSchneider; Kawashima, E.; N, D.; Jones, G.; Dalke, A.; Cole, B.; Swain, M.; Turk, S.; AlexanderSavelyev; Vaucher, A.; Wójcikowski, M.; Ichiru Take; Probst, D.; Ujihara, K.; Scalfani, V. F.; Godin, G.; Lehtivarjo, J.; Walker, R.; Pahl, A.; Francois Berenger; Jasondbiggs; Strets123. Rdkit/Rdkit: 2023_03_3 (Q1 2023) Release, 2023. https://doi.org/10.5281/ZENODO.8254217.
(53) OEChem TK. 2.2.2. OpenEye, Cadence Molecular Sciences, Santa Fe, NM. Http://Www.Eyesopen.Com.
(54) Omega TK 2.2.2. OpenEye, Cadence Molecular Sciences, Santa Fe, NM. Http://Www.Eyesopen.Com.
(55) Pearce, N. M.; Krojer, T.; Bradley, A. R.; Collins, P.; Nowak, R. P.; Talon, R.; Marsden, B. D.; Kelm, S.; Shi, J.; Deane, C. M.; Von Delft, F. A Multi-Crystal Method for Extracting Obscured Crystallographic States from Conventionally Uninterpretable Electron Density. *Nat. Commun.* **2017**, *8* (1), 15123. https://doi.org/10.1038/ncomms15123.
(56) Mueller, U.; Förster, R.; Hellmig, M.; Huschmann, F. U.; Kastner, A.; Malecki, P.; Pühringer, S.; Röwer, M.; Sparta, K.; Steffien, M.; Ühlein, M.; Wilk, P.; Weiss, M. S. The Macromolecular Crystallography Beamlines at BESSY II of the Helmholtz-Zentrum Berlin: Current Status and Perspectives. *Eur. Phys. J. Plus* **2015**, *130* (7), 141. https://doi.org/10.1140/epjp/i2015-15141-2.
(57) Sparta, K. M.; Krug, M.; Heinemann, U.; Mueller, U.; Weiss, M. S. *XDSAPP2.0*. *J. Appl. Crystallogr.* **2016**, *49* (3), 1085–1092. https://doi.org/10.1107/S1600576716004416.
(58) Schiebel, J.; Krimmer, S. G.; Röwer, K.; Knörlein, A.; Wang, X.; Park, A. Y.; Stieler, M.; Ehrmann, F. R.; Fu, K.; Radeva, N.; Krug, M.; Huschmann, F. U.; Glöckner, S.; Weiss, M. S.; Mueller, U.; Klebe, G.; Heine, A. High-Throughput Crystallography: Reliable and Efficient Identification of Fragment Hits. *Structure* **2016**, *24* (8), 1398–1409. https://doi.org/10.1016/j.str.2016.06.010.
(59) Wojdyr, M.; Keegan, R.; Winter, G.; Ashton, A. *DIMPLE* - a Pipeline for the Rapid Generation of Difference Maps from Protein Crystals with Putatively Bound Ligands. *Acta Crystallogr. A* **2013**, *69* (a1), s299–s299. https://doi.org/10.1107/S0108767313097419.
(60) Füsser, F. T.; Koch, O.; Kümmel, D. Crystal Structure of Mycobacterium Smegmatis Thioredoxin Reductase, 2023. https://doi.org/10.2210/pdb8CCI/pdb.